1 # Depletion of atmospheric gaseous elemental mercury by plant uptake at

2 # Mt. Changbai, Northeast China

3   Xuewu Fu[1], Wei Zhu[1], Hui Zhang[1], Jonas Sommar[1], Xu Yang[1], Xun Wang[1,2], Che-Jen Lin[1,3,4], Xinbin Feng[1,*]

4   [1]State Key Laboratory of Environmental Geochemistry, Institute of Geochemistry, Chinese Academy of Sciences, 99

5   Lincheng West Road, Guiyang, 550081, China

6   [2]University of the Chinese Academy of Sciences, Beijing 100049, China

7   [3]Department of Civil and Environmental Engineering, Lamar University, Beaumont, Texas 77710, United States

8   [4]Center for Advances in Water and Air Quality, Lamar University, Beaumont, Texas 77710, United States

10   Correspondence to:Xinbin Feng (fengxinbin@vip.skleg.cn)

13   Abstract: There exists observational evidence that GEM can be readily removed from the

14   atmosphere via chemical oxidation followed by deposition in the polar and sub-polar regions,

15   free troposphere, lower stratosphere, and marine boundary layer under specific environmental

16   conditions. Here we report GEM depletions in a temperate mixed forest at Mt. Changbai,

17   Northeast China. The depletion occurred exclusively at night during leaf-growing season and in

18   the absence of GOM enrichment (GOM < 3 pg m^{-3}). Vertical gradients of decreasing GEM

19   concentrations from layers above to under forest canopy suggest in situ loss of GEM to forest

20   canopy at Mt. Changbai. Foliar GEM flux measurements showed that the foliage of two

21   predominant tree species is a net sink of GEM at night, with a mean deposition flux of -1.8 ± 0.3

22   ng m^2 h^{-1} over *Fraxinus mandshurica* (deciduous tree species) and -0.1 ± 0.2 ng m^2 h^{-1} over

23   *Pinus Koraiensis* (evergreen tree species). Daily integrated GEM δ^{202}Hg, Δ^{199}Hg, and Δ^{200}Hg at

24   Mt. Changbai ranged from -0.34 to 0.91‰, from -0.11 to -0.04‰ and from -0.06 to 0.01‰,

25   respectively. A large positive shift of GEM δ^{202}Hg occurred during the GEM depletion events,

26   whereas Δ^{199}Hg and Δ^{200}Hg remained essentially unchanged. The observational findings and box

27   model results show that uptake of GEM by forest canopy plays a predominant role in the GEM

28   depletion at Mt. Changbai forest. Such depletion events of GEM are likely to be a widespread

29   phenomenon, suggesting that the forest ecosystem represents one of the largest sinks (~1930 Mg)

30   of atmospheric Hg at global scale.

32

1 Introduction

Mercury (Hg) is a persistent toxic air pollutant that is ubiquitously distributed in the atmosphere. There are three operationally defined Hg forms: gaseous elemental mercury (GEM), particulate bound mercury (PBM), and gaseous oxidized mercury (GOM). The sum of GEM and GOM is known as total gaseous mercury (TGM). Because of its mild reactivity, high volatility, low dry deposition velocity and water solubility, GEM is the most abundant form of Hg in the atmosphere (Gustin and Jaffe, 2010;Holmes et al., 2010). The cycling of GEM in the atmosphere is largely depending on either direct dry deposition or chemical oxidation followed by wet and dry deposition. The residence time of GEM in the atmosphere is estimated to be in the range of 0.5 - 2.0 yr, based on global Hg budget and empirical models (Lindberg et al., 2007). Over the past decades, our understanding regarding the sources and sinks of atmospheric Hg has been improved (Strode et al., 2007;Selin et al., 2008;Holmes et al., 2010;Amos et al., 2013). For instance, the discovery of atmospheric mercury depletion events (AMDEs) in polar and sub-polar regions demonstrated that atmospheric GEM can be readily removed from the atmosphere via reactive halogens-induced oxidation, leading to a deposition of up to 300 Mg yr^{-1} to the arctic (Schroeder et al., 1998;Ebinghaus et al., 2002;Lindberg et al., 2002;Steffen et al., 2008). Similar depletion events occurred in the marine boundary layer at middle latitude to a lesser extent (Brunke et al., 2010;Obrist et al., 2011;Timonen et al., 2013). Fast oxidation of GEM by ozone, reactive halogens and hydroxyl radicals in the free troposphere has also been observed (Swartzendruber et al., 2006;Fain et al., 2009;Swartzendruber et al., 2009b;Lyman and Jaffe, 2012;Shah et al., 2016). These findings indicate that GEM probably has a much shorter atmospheric residence time under specific environmental conditions (Holmes et al., 2010). Dry deposition of GEM (V_d) depends on surface characteristics, meteorological variables, biological and chemical conditions of soil and water. V_d over non-vegetated surfaces (bare soil) and water bodies is typically small (less than 0.03 cm s^{-1}) to counter the emission and re-emission of GEM from these surfaces (Zhang et al., 2009). Therefore soil and water have long been considered a net GEM source (Selin et al., 2007;Holmes et al., 2010). In contrast, strong dry deposition of

60 GEM to vegetated surfaces and wetlands are frequently observed with V_d up to about 2 cm s^{-1}

61 (Zhang et al., 2009), suggesting vegetative surfaces an important sink of GEM.

62   Forest represents a dominant terrestrial ecosystem on the Earth and covers an area of

63 $\sim 4 \times 10^7$ km^2. It readily removes trace gases such as CO_2, ozone, sulfur dioxide, and nitrogen

64 oxides, as well as aerosols from the atmosphere (Munger et al., 1996;Finkelstein et al.,

65 2000;Zhang et al., 2001;Pan et al., 2011). However, there are ongoing debates regarding whether

66 or not forest is a sink or a source of atmospheric Hg. Previous laboratory studies suggested that

67 foliar exchange of GEM is bi-directional with net deposition occurring at elevated Hg

68 concentration and net emission under typical background concentrations (Hanson et al.,

69 1995;Ericksen and Gustin, 2004;Gustin et al., 2004;Graydon et al., 2006). Lindberg et al. (1998)

70 measured GEM fluxes over a mature deciduous forest using the modified Bowen ratio (MBR)

71 method and suggested that global forest is a net source of GEM with an emission ranging from

72 850 to 2000 Mg yr^{-1}. Later, the observation of Hg fluxes in a deciduous forest using a relaxed

73 eddy accumulation (REA) method showed seasonal shift in flux with a net deposition of GEM

74 during leaf-growing season (Bash and Miller, 2009). Although the discrepancy in the measured

75 GEM exchanges between forest and atmosphere is partially attributed to the uncertainties of the

76 flux quantification method (Sommar et al., 2013), there is a need to clarify the role of forest

77 ecosystem in the mass budget of atmospheric GEM. A study in Québec, Canada showed that

78 GEM concentrations at a maple forest site are consistently lower than those measured at an

79 adjacent open site (Poissant et al., 2008). Similarly, the lower GEM concentrations observed in

80 leaf-growing season at many forest sites across the Atmospheric Mercury Network (AMNet) in

81 USA (Lan et al., 2012) also suggest forest a net GEM sink. Currently, it is still unclear whether

82 the loss of GEM over forest is caused by direct dry deposition to canopy or chemical

83 conversions of GEM to GOM (Mao et al., 2008).

84   In this study, we report consistent GEM depletion events during the leaf-growing season in

85 a temperate mixed forest in Northeast China over a time scale of 7 years. Atmospheric Hg

86 speciation, vertical gradient of GEM, foliage/air and soil/air exchange flux of GEM and isotope

87 signatures of GEM samples have also been observed in an intensive campaign to explore the

88 possible mechanisms responsible for the observed GEM depletion.

2 Material and Methods

2.1 Site description

91 The study site (42º24′0.1″N, 128º 06′25″E, 738 m above sea level) is located in a temperate

92 broadleaf and Korean pine mixed forest on the north slope of Mt. Changbai (Figure S1). The

93 forest is dominated by tree species of *Pinus koraiensis*, *Fraxinus mandshurica*, *Tilia amurensis*,

94 *Acer mono* and *Quercus mongolica*. The height of the forest canopy is 5 - 22 m (mean = 18.3 m)

95 with the heights of mature trees (>50 y) and young trees (<20 y) and shrubs ranging from 15 to

96 22 m and from 5 to 10 m, respectively. Regions to the east and south of the site consist of

97 pristine forest with little anthropogenic influence. Most of the regional industrial sources are

98 located more than 50 km west of the sampling site (Supplementary Figure S1).

2.2 Atmospheric Hg measurements

100 From Oct 2008 to Jul 2013 and from Jul 2014 to Dec 2015, TGM concentrations were

101 continuously measured using an automated Hg vapor analyzer (Tekran® 2537, Tekran Inc.,

102 Canada). The analyzer has been used extensively for atmospheric TGM measurements

103 worldwide. The analyzer was calibrated automatically every 25 h using the internal Hg^0

104 permeation source. The permeation rate of the internal source was manually calibrated every 4 -

105 6 months by using an external Hg vapor source (Tekran® 2505). The sampling inlet was

106 mounted at a height of 24 m above ground level (agl, ~3 m above canopy) by using a 25 m

107 Teflon tube and a 15 m heated Teflon tube. Atmospheric TGM consists of GEM and GOM.

108 Gustin et al. (2013;2015) proposed that GOM could be transformed to GEM within the

109 uncovered Teflon tubing, which in turn would be transported efficiently through the tubing and

110 quantified by the Tekran analyzer. However, GOM generally constitutes a small portion of TGM

111 (mean of 0.32% on basis of one year of measurements and will not exceed 1% using a three-fold

112 correction factor to adjust GOM concentrations measured by the Tekran® speciated system)

113   (Gustin et al., 2015). Therefore, we interpret the TGM observations as GEM throughout the

114   paper.

115   GEM, GOM and PBM were measured using the Tekran® 2537/1130/1135 unit (Tekran Inc.,

116   Canada) from Jul 2013 to Jul 2014. The sampling inlet was positioned at 4 m agl in a small

117   clearing plot with tall trees of ~5 m from the system. This system has been widely used and

118   described in detail by many earlier studies (Landis et al., 2002;Lindberg et al., 2002;Lan et al.,

119   2012;Fu et al., 2016). Briefly, GOM, PBM, and GEM in ambient air were collected onto

120   KCl-coated annular denuder, quartz fiber filter and dual gold cartridges in sequence. This system

121   was programmed to collect GOM and PBM at 1-h intervals at a volumetric flow rate of 10 L

122   min^{-1}. GEM was collected from air samples at 5-min intervals at a volumetric flow rate of 1.0 L

123   min^{-1}. Once collected, Hg is thermally decomposed from each unit and detected by cold vapor

124   atomic fluorescence spectroscopy (CVAFS) as Hg^{0}. KCl-coated denuder, Teflon coated glass

125   inlet, and impactor plate were replaced bi-weekly and quartz filters were replaced monthly.

126   Denuders and quartz filters were prepared and cleaned before field sampling following the

127   methods in Tekran technical notes. GEM concentrations measured at 4 m agl in the small

128   clearing plot and at 45 m agl (~24 m above canopy) did not bias significantly with each other

129   with a mean difference of 0.03 ng m^{-3} (3% of the mean GEM concentration during the study

130   period) (Supplementary Figure S2). The two Tekran instruments used for this comparison were

131   run side by side for 2 days in the laboratory and showed a mean systematic uncertainty of 1.8 ±

132   1.1% (ranging from 0% to 5.7%). This indicates the measurements at 4 m agl in the small

133   clearing plot did not significantly underestimate the GEM concentrations of ambient air in the

134   study area. In the study area, GEM also has a fast dry deposition velocity within the forest (more

135   details in sections below), although to a lesser extent compared to atmospheric GOM. We

136   therefore assume that the measurements of GOM in the clearing plot didn't result in significantly

137   biased low GOM concentrations and were representative of ambient air in the study area.

138   Vertical profile of GEM concentrations at 1 m, 10 m, 24 m, and 45 m agl within the forest

139   were measured from 10 to 15 Jul 2013 using the Tekran® 2537 analyzer and the Tekran® 1115

140   Synchronized Multi-Port manifold (Tekran Inc., Canada). The sampling duration of GEM during

141   the vertical gradient measurements was programmed to be 2.5 min, and switching of ports of the

142   manifold was made every 5 min.

143   The GEM detection limit for 7.5 L samples measured with Tekran® 2537 analyzer as

144   specified by Tekran Instrument Corporation is 0.1 ng m^{-3}. Due to the lack of understanding of

145   the specific forms and calibration standards of GOM, there are uncertainties regarding the GOM

146   measurements (Gustin et al., 2015). Previous studies suggested that GOM measured by the

147   Tekran system could be biased low and a correction factor of 3 should be applied for adjusting

148   GOM concentrations measured by the Tekran system (Gustin et al., 2013;Huang et al.,

149   2013;Gustin et al., 2015;Huang and Gustin, 2015). Tekran® 2537's default integration at low Hg

150   loading (~1 pg per cycle) was reported to have a 25% underestimation of GEM concentration.

151   This could also underestimate GOM concentrations when GOM concentrations were lower than

152   2 pg m^{-3} (Swartzendruber et al., 2009a). These analytical uncertainties are taken into account for

153   the discussions of GEM depletion mechanism in the Results and Discussion section.

154   **2.3 Foliar GEM exchange**

155   Exchange flux of GEM between leaf and the atmosphere was measured using a new

156   dynamic flux bag method described by Graydon et al. (2006) which is thought to maintain

157   normal physiological function of enclosed foliage. Briefly, a Tedlar® gas sampling bag (~20 L

158   volume, polyvinyl fluoride, DuPont, USA) enclosed living intact leaves, and the foliar GEM flux

159   was obtained via measuring the difference in GEM concentrations at the inlet and outlet of the

160   flux bag. Ambient air was pumped into the flux bag using a Mini Diaphragm vacuum pump

161   (N89 KTDC, KNF, Germany, oil-free, brushless and with diaphragm coated with PTFE). GEM

162   flux was calculated using Equation (1):

163   $$F=(C_o-C_i)\times Q/A \quad (1)$$

164   where F is the foliar GEM flux in ng m^{-2} h^{-1}, with positive and negative fluxes representing

165   emission and deposition, respectively, C_o and C_i are the GEM concentrations at the outlet and

166   inlet of the flux bag, respectively, which were measured by the Tekran® 2537 analyzer, Q is the

167   flushing flow rate of air through the flux bag (0.5 m^3 h^{-1}), and A is the single-sided leaf area

168   enclosed by the flux bag in m^2.

169   Two tree species, *Fraxinus mandshurica* (deciduous tree species) and *Pinus Koraiensis*

170   (evergreen tree species), were selected for the foliar GEM flux measurement. They are the

171   predominant species in the study area with the basal coverage of the *Fraxinus Mandschurica*

172   and *Pinus Koraiensis* accounting for 26.3% and 27.5% of the total basal area (Dai et al., 2011).

173   Both selected species for flux measurement are mature with a height of ~20 m. The flux bag

174   was installed at the height of 15 m agl. Foliar GEM fluxes over *Fraxinus mandshurica* and

175   *Pinus Koraiensis* were continuously measured during 16-17 and 17-18 Jul 2013, respectively,

176   and 24-h continuous flux data were obtained for each species. Mean blank of flux chamber

177   measured before and after the field experiment was -0.02 ± 0.04 ng m^{-2} h^{-1} (n=24), which was

178   indistinguishable from zero and not used to calibrate the measured fluxes.

2.4 Isotopic Composition of Atmospheric GEM

180   From 8 to 18 July 2013, GEM samples were collected at 4 m agl at the study site for Hg

181   isotopes analysis using a chlorine-impregnated activated carbon (CLC) trap (Fu et al., 2014).

182   Atmospheric GEM was collected daily (24-h sampling duration) at a flow rate of 10 LPM. CLC

183   traps collect GEM at >95% efficiency at the given sampling flow rate (Fu et al., 2014). To

184   remove air particles, a 47-mm diameter Teflon filter (pore size 0.2 μm) was installed at the inlet

185   of CLC trap. The CLC trap was kept warm (50 - 70 °C) during sampling using a silicone rubber

186   heating pads (RadioSpares) to prevent water condensation. The sampling flow rate of CLC

187   traps was regulated via a gas flow meter installed at the outlet of the vacuum pump, and the

188   total sampling volumes of the CLC traps were recorded using a gas meter, calibrated to

189   standard volumes under a standard pressure of 1013 hPa and a standard temperature of 273.14

190   K using a Bios Defender.

191   After the completion of field sampling, CLC traps were sealed with silicone stoppers and

192   three successive polyethylene bags and stored in a clean environment until pre-concentration

193   into trap solutions for Hg isotope analysis. GEM collected by CLC traps were preconcentrated

194   into reverse aqua regia solution (v/v, $2HNO_3/1HCl$) in the laboratory using a double-stage

195   combustion protocol for Hg isotope analysis (Biswas et al., 2008;Sun et al., 2013;Fu et al.,

196   2014). Hg isotope ratios were determined by Nu-Plasma MC-ICP-MS following a previously

197   established method (Yin et al., 2013). Hg isotopic composition is reported in delta notation (δ)

198   in per mil referenced to the bracketed NIST 3133 Hg standard (Blum and Bergquist, 2007):

199
$$\delta^{xxx}Hg = \left(\frac{\left(\frac{xxx_{Hg}}{198_{Hg}}\right)_{sample}}{\left(\frac{xxx_{Hg}}{198_{Hg}}\right)_{SRM3133}} - 1 \right) \times 1000‰ \qquad (2)$$

200   Mass independent fractionation (MIF) values are expressed by "capital delta (Δ)" notation

201   (‰), which is the difference between the measured values of $\delta^{199}Hg$, $\delta^{200}Hg$, $\delta^{201}Hg$ and those

202   predicted from $\delta^{202}Hg$ using the kinetic MDF law (Blum and Bergquist, 2007):

203                  $\Delta^{199}Hg$ (‰) = $\delta^{199}Hg$ - ($0.252 \times \delta^{202}Hg$)   (3)

204                   $\Delta^{200}Hg$ (‰) = $\delta^{200}Hg$ - ($0.502 \times \delta^{202}Hg$)   (4)

205                   $\Delta^{201}Hg$ (‰) = $\delta^{201}Hg$ - ($0.752 \times \delta^{202}Hg$)   (5)

206   The analytical uncertainty of isotopic analysis was obtained by repeated analysis of the

207   UM-Almaden standard. The overall mean values of $\delta^{202}Hg$ and $\Delta^{199}Hg$ for all the UM-Almaden

208   standards were -0.57 ± 0.09 ‰ and -0.03 ± 0.04 ‰ (2SD, n = 12), respectively, consistent with

209   previously reported values (Blum and Bergquist, 2007). In the present study, the analytical

210   uncertainty of CV-MC-ICPMS isotope analysis is the 2SD uncertainty of the UM-Almaden

211   standard, unless the 2SD uncertainty on repeated analysis of the same sample over different

212   analytical sessions is larger.

213   **3 Results and discussion**

214   **3.1 Characteristics of depletion events at Mt. Changbai**

215   From Oct 2008 to Dec 2015, we observed 52 depletion events with dips of GEM

216   concentrations <0.5 ng m^{-3}. These depletions occurred predominantly from May to September

217   (Figure 1). GEM concentrations during a typical depletion event decreased rapidly from ~1.50

218   ng m^{-3} around noon to <0.5 ng m^{-3} at night, corresponding to >65% loss of GEM. Figure 2 shows

219   the representative depletion events in summer of 2010 and 2013. Strong depletion of GEM

220   consistently occurred at night. During the 7 - 13 July, 2010 period, a nearly complete depletion

221   occurred with GEM concentrations decreasing from 1.6 - 2.0 ng m^{-3} at noon to nearly zero at

222   night (removal of GEM averaged 1.83 ± 0.35 ng m^{-3} (n = 7)). The daytime peak GEM

223   concentrations for the depletion events during 9 - 23 Jul, 2013 ranged from 1.50 - 2.31 ng m^{-3},

224   and the lowest GEM concentrations at night were 0.35 - 0.99 ng m^{-3}, yielding an averaged

225   removal of GEM of 1.08 ± 0.23 ng m^{-3} (n = 12).

226   GOM concentrations during the nighttime atmospheric GEM depletion events (n = 10,

227   defined as nighttime dips in GEM concentrations <0.5 ng m^{-3}) from Jul 2013 to Jul 2014 were

228   typically low (< 3 pg m^{-3} with a mean value of 0.8 pg m^{-3}). This is in contrast to previously

229   characterized GEM depletions in the polar and sub-polar regions, marine boundary layer and

230   free troposphere where depletions of GEM were accompanied by strong GOM enhancements

231   (up to 195 - 1200 pg m^{-3}) (Lindberg et al., 2002;Swartzendruber et al., 2006;Sheu et al.,

232   2010;Obrist et al., 2011;Lyman and Jaffe, 2012). Wind speed was low (mean of 0.1 m s^{-1} during

233   7 - 13 Jul, 2010 and 0.4 m s^{-1} during 9 - 23 Jul, 2013) during the nighttime depletion events at

234   the study site (Figure 2). Shallow nocturnal boundary layer (NBL, see text in the SI) was

235   frequently developed when the depletion occurred with a mean height of 146 m (74 - 200 m)

236   during 7 - 13 Jul, 2010 and 209 m (57 - 300 m) during 9-23, Jul, 2013 (Figure 2). The low winds

237   and shallow NBL limited the transport of air masses at the sampling site and facilitated a

238   continuous depletion of GEM in the presence of vegetative uptake of GEM (more details in

239   sections below). During daytime, the surface wind speed and NBL depth increase due to solar

240   heating (Talbot et al., 2005), enabling the downward transport of GEM from upper air, resulting

241   in the increasing GEM concentrations.

242   Summer nighttime depletion of GEM has also been observed at forest sites in North

243   America (e.g., St. Anicet Maple forest station in Canada, and Piney Reservoir, Huntington

244   Wildlife, Thompson Farm, Kejimkujik National Park, and Stilwell in AMNet, USA) (Mao et al.,

245   2008;Poissant et al., 2008;Lan et al., 2012). Such depletion of GEM in forest ecosystems is

246   likely a widespread phenomenon globally. The depletion at forest sites was different from the

247   atmospheric mercury depletion events (AMDEs) elsewhere. For instance, the AMDEs at Cape

248   Point, coast of South Africa and Dead Sea, Israel are mostly observed during daytime (Brunke et

249   al., 2010;Obrist et al., 2011). The AMDEs in the Polar Regions occur exclusively during Polar

250   sunrise in spring and do not exhibit a well-defined diurnal pattern (Schroeder et al.,

251   1998;Ebinghaus et al., 2002;Lindberg et al., 2002).

252   3.2 Vertical gradient of GEM observed at Mt. Changbai

253   A clear vertical gradient of GEM concentrations was observed at the study site, with

254   increasing GEM concentrations with respect to sampling altitude (Figure 3). The average

255   difference in GEM concentrations between 45 m and 1 m (all in agl, ΔGEM_{45-1m}) was 0.22 ±

256   0.15 ng m^{-3} (n = 330), ~20% of the mean GEM concentration at 45 m agl. Average differences in

257   GEM concentrations between 45 m and 24 m (ΔGEM_{45-24m}), between 24 m and 10 m

258   (ΔGEM_{24-10m}), and between 10 m and 1 m (ΔGEM_{10-1m}) were 0.11 ± 0.10, 0.05 ± 0.09, and 0.06

259   ± 0.11 ng m^{-3} (n = 330), respectively. The observed gradient suggested that the forest at the study

260   site is a net sink for atmospheric GEM, in contrast to the vertical GEM gradients observed in a

261   mature hardwood forest (between 30 and 40 m agl) in Walker Branch Watershed, Tennessee,

262   USA during daytime, which showed decreasing GEM concentrations with sampling altitude

263   above the forest canopy (Lindberg et al., 1998). This difference might be caused by the different

264   forest structure and elevated emission flux of GEM from forest soil (7.5 ng m^{-2} h^{-1} in Walker

265   Branch Watershed versus 2.8 ng m^{-2} h^{-1} at Mt. Changbai, Supplementary Figure S3) in Walker

266   Branch Watershed (Kim et al., 1995;Lindberg et al., 1998).

267   The vertical gradients of GEM at Mt. Changbai showed clear diurnal trends (Figure 3 and

268   Supplementary Figure S4). ΔGEM_{45-24m} and ΔGEM_{24-10m} values were comparably higher at night

269   (mean = 0.13 and 0.08 ng m^{-3}) than those during daytime (0.09 and 0.02 ng m^{-3}). The smaller

270   daytime ΔGEM_{45-24m} and ΔGEM_{24-10m} were a result of weaker dry deposition of GEM to the

271   forest canopy (more discussion later). A strong negative correlation between the ΔGEM_{24-10m} and

272   wind speed (r^2 = 0.55, p<0.01) also suggested stronger vertical mixing during daytime inhibited

273 the buildup of GEM gradient. The diurnal trend of ΔGEM_{10-1m} was opposite to ΔGEM_{45-24m} and

274 ΔGEM_{24-10m}, with larger values during daytime (mean = 0.09 ng m^{-3}) and lower values at night

275 (mean = 0.04 ng m^{-3}).

3.3 Foliage/air exchange flux of GEM

277 Mean foliar GEM fluxes over *Fraxinus Mandschurica* and *Pinus Koraiensis* were -1.2 ±

278 0.6 (-2.2 to -0.2 ng m^{-2} h^{-1}) and 0.0 ± 0.4 ng m^{-2} h^{-1} (-0.5 to 2.0 ng m^{-2} h^{-1}), respectively (Figure

279 4). Mean ambient GEM concentrations during the flux measurements over *Fraxinus*

280 *Mandschurica* and *Pinus Koraiensis* were 1.42 ± 0.23 and 0.93 ± 0.28 ng m^{-3}, respectively,

281 below the background concentrations of GEM in the Northern Hemisphere (1.5 - 1.7 ng m^{-3})

282 (Lindberg et al., 2007). The low GEM deposition flux over *Pinus Koraiensis* was partially

283 attributed to the low ambient GEM concentration that weaken the deposition flux (Hanson et al.,

284 1995;Ericksen and Gustin, 2004). The mean deposition fluxes over *Fraxinus Mandschurica* (0.7

285 ± 0.1 ng m^{-2} h^{-1}) was much greater than the that over *Pinus Koraiensis* (0.0 ± 0.5 ng m^{-2} h^{-1})

286 given the same GEM (1.0 – 1.4 ng m^{-3}) range (Figure 4), suggesting that GEM deposition flux

287 varies with tree species with deciduous tree species inducing higher deposition compared to

288 evergreen tree species (Millhollen et al., 2006).

289 The observed foliar GEM fluxes over *Fraxinus Mandschurica* and *Pinus Koraiensis* were

290 within the range of reported values (means = -6 to 3.5 ng m^{-2} h^{-1}) (Ericksen et al.,

291 2003;Frescholtz and Gustin, 2004;Gustin et al., 2004;Graydon et al., 2006;Poissant et al.,

292 2008;Stamenkovic and Gustin, 2009). A diurnal pattern with higher deposition fluxes at night

293 was observed for both species. The higher deposition flux at night can be attributed to enhanced

294 foliar GEM uptakes. As seen in Figure 4, GEM concentrations in the outlet stream of the flux

295 bag over *Fraxinus Mandschurica* showed a remarkable decline at night compare to daytime

296 (mean GEM$_{outlet-night}$ = 0.28 ± 0.11 ng m^{-3}, mean GEM$_{outlet-daytime}$ = 0.75 ± 0.08 ng m^{-3}). It has

297 been suggested that lower O$_3$ and higher relative humidity (RH) could facilitate the uptake of

298 GEM by foliage (Lindberg and Stratton, 1998;Stamenkovic and Gustin, 2009). O$_3$ and RH at the

299 study site showed strong diurnal patterns with decreasing O$_3$ concentrations and increasing RH at

300   night (Supplementary Figure S5), which may explain the higher deposition fluxes of GEM to

301   foliage at night. Both stomatal and non-stomatal uptakes have been suggested to be responsible

302   for the observed foliage-atmosphere GEM exchange (Zhang et al., 2005;Stamenkovic and

303   Gustin, 2009). Stamenkovic and Gustin (2009) found that GEM deposition flux to foliage

304   remained essentially unchanged whether or not stomata are open. This indicates that

305   non-stomatal route plays an important role in the uptake of GEM by foliage, consistent with the

306   observations in this study. Foliar exchange of GEM is bi-directional with foliage emitting GEM

307   at global background air GEM concentrations (Hanson et al., 1995;Ericksen and Gustin,

308   2004;Graydon et al., 2006). With the GEM concentrations in the range of 0.41 – 1.82 ng m^{-3}

309   during this study, however, net deposition was observed except for *Pinus Koraiensis* during

310   daytime when stoma are open. Net emission of GEM from *Pinus Koraiensis* during daytime

311   could be attributed to the enhanced photochemical reduction and re-emission of previously

312   deposited Hg (GEM, GOM and PBM), Hg in dew water and transpiration stream as well as

313   transpiration of Hg^0 in soil pores (Bishop et al., 1998;Lindberg et al., 1998;Ericksen and Gustin,

314   2004;Stamenkovic and Gustin, 2009).

315   The observed foliar GEM fluxes over *Fraxinus Mandschurica* were negatively correlated

316   with the GEM concentrations in the inlet air (Figure 5A), yielding a compensation point of 0.52

317   ng m^{-3} during daytime and 0.47 ng m^{-3} during nighttime, respectively. No correlation between

318   foliar GEM fluxes and ambient GEM concentrations was observed for *Pinus Koraiensis* during

319   daytime. However, a negative correlation was observed at night when ambient GEM

320   concentrations were higher than 0.98 ng m^{-3} (Figure 5B), which was likely the compensation

321   point for *Pinus Koraiensis* during nighttime. These observed compensation points were

322   comparatively lower than the values (2 - 3 ng m^{-3}) measured in laboratory studies (Ericksen and

323   Gustin, 2004;Graydon et al., 2006), but consistent with the field observation at St. Anicet Maple

324   forest, Canada (0.53 ng m^{-3}) (Poissant et al., 2008). For *Pinus Koraiensis*, the observed foliar

325   GEM fluxes were not significantly different from zero (mean = -0.1 ± 0.1 ng m^{-2} h^{-1}) at GEM

326   concentrations lower than the compensation point (0.98 ng m^{-3}). A similar conclusion cannot be

327   reached for *Fraxinus Mandschurica* because the ambient GEM concentrations were higher than

328   the respective compensation points during the entire campaign (Figure 5A). This finding is

329   different from previous results that showed net GEM emissions from foliage at ambient GEM

330   concentrations below the compensation points (Hanson et al., 1995;Graydon et al.,

331   2006;Poissant et al., 2008). Based on the field findings, it is likely that the uptake and emission

332   of GEM over the foliage of *Pinus Koraiensis* reached equilibrium during nighttime when the

333   ambient GEM concentrations were below the compensation point.

334   The total deposition flux of GEM to forest canopy at Mt. Changbai was estimated using

335   Equation (6):

336 $$F = LAI \times \sum_{i}^{n}(F_i \times A_i) \qquad (6)$$

337   where F is the total deposition flux of GEM in ng m^{-2} h^{-1}, LAI is the mean leaf area index

338   (dimensionless), F_i is the foliar GEM flux of a tree species (i) in ng m^{-2} h^{-1}, and A_i is the relative

339   basal area of a tree species (i) in percentile (Dai et al., 2011). In this study, it is assumed that the

340   measured mean foliar GEM fluxes over *Fraxinus Mandschurica* and *Pinus Koraiensis* are

341   representative of deciduous tree species and evergreen tree species, respectively. The measured

342   mean LAI at Mt. Changbai during leaf-growing season was 5.4.

343   The total deposition fluxes of GEM to forest canopy at Mt. Changbai during nighttime and

344   daytime are estimated to be 7.3 (V_d of 0.14 cm s^{-1}) and 2.5 ng m^{-2} h^{-1} (V_d of 0.04 cm s^{-1}). We

345   acknowledge that, due to the relatively short field sampling periods for the two selected tree

346   species and the fact that foliar GEM flux may vary with tree species, GEM concentrations and

347   other environmental variables, our estimates may have large uncertainties. Nevertheless, the

348   estimates are generally consistent with the measured deposition flux using Hg accumulated in

349   foliage over time. The mean mass-weighted Hg concentration in litter samples at the study site

350   was 43.0 ± 29.5 ng g^{-1} (Supplementary Table S1). With the annual litterfall of 486 g m^{-2} at the

351   site (Zhou et al., 2014), the Hg deposition flux in litterfall was 20.9 ± 14.3 μg m^{-2} yr^{-1}. Assuming

352   that the plant foliage had a constant uptake rate of Hg in the leaf-growing season (from May to

353   September), the hourly deposition flux of Hg that end up being contained in litterfall would be

354 5.7 ng m^{-2} h^{-1}, comparable to the GEM deposition flux calculated from flux bag observations

355 (daily mean: 4.9 ng m^{-2} h^{-1}).

3.4 Mechanisms for the observed GEM depletion

357   Oxidation of GEM by reactive halogens and O$_3$ has been proposed to be an important

358 mechanism for GEM depletions observed elsewhere as evidenced by the elevated GOM

359 concentrations (up to 500 - 1200 pg m^{-3}) associated with the GEM depletion events and an

360 inverse correlation between GOM and GEM concentrations (Lindberg et al., 2002;Obrist et al.,

361 2011;Lyman and Jaffe, 2012). Based on modeling assessments, the nighttime loss of GEM in

362 forest areas has been suggested to be caused by dry deposition and chemical oxidation (by ozone,

363 OH and NO$_3$) (Mao et al., 2008). However, the GOM concentrations observed during typical

364 nighttime GEM depletion events at Mt. Changbai were extremely low (< 3 pg m^{-3} with a mean

365 value of 0.8 pg m^{-3}), similar to those observed at other forest sites (Piney Reservoir, Huntington

366 Wildlife, Thompson Farm, Kejimkujik National Park, and Stilwell) in North America (means =

367 0.5 - 4 pg m^{-3} at summertime night) (Lan et al., 2012). In addition, concentrations of many

368 atmospheric oxidants (e.g., O$_3$, OH, NO$_3$, BrO) at global forest sites were low (Spivakovsky et

369 al., 2000;Yang et al., 2005;Rinne et al., 2012;Hens et al., 2014), which does not support

370 significant conversion of GEM to GOM. Given the environmental condition at Mt. Changbai,

371 the dry deposition flux of GOM was estimated to be 0.034 ng m^{-2} h^{-1}, using the mean nighttime

372 GOM concentration (0.8 pg m^{-3}) measured during the GEM depletion events and reported V_d of

373 GOM (0.1 to 5.9 cm s^{-1} with a mean of 1.2 cm s^{-1}) to forest canopy (Lindberg and Stratton,

374 1998;Rea et al., 2000;Zhang et al., 2012). Even with a correction factor of 3 to account for the

375 potential under-estimation of GOM concentration by the Tekran® speciation system (Gustin et

376 al., 2013;Huang et al., 2013;Gustin et al., 2015), the deposition flux contributed by GOM is 0.1

377 ng m^{-2} h^{-1}. Assuming that all GOM was formed through in situ oxidation of GEM, the chemical

378 pathway would contribute to merely 1.4% of the measured deposition flux of GEM to forest

379 canopy during the nighttime depletion events.

380   Measurements of GEM isotopic composition also provided insight into the mechanisms

381   responsible for the GEM depletion at Mt. Changbai. $\delta^{202}Hg$, $\Delta^{199}Hg$, and $\Delta^{200}Hg$ of the daily

382   GEM samples from 8 to 18 Jul 2013 were -0.34 to 0.91‰, -0.11 to -0.04‰ and -0.06 to 0.01‰,

383   respectively (n=10, Figure 6, Supplementary Table S2). These are consistent with the

384   observations in the Great Lakes region, Barrow, Alaska, Pensacola, FL and Wisconsin forest in

385   USA ($\delta^{202}Hg_{GEM}$ = -0.12 to 1.43‰, $\Delta^{199}Hg_{GEM}$ = -0.31 to -0.01‰, $\Delta^{200}Hg$ = -0.11 to 0.1‰)

386   (Gratz et al., 2010;Sherman et al., 2010;Demers et al., 2013;Demers et al., 2015). A large

387   positive $\delta^{202}Hg_{GEM}$ shift was associated with strong GEM depletions; whereas $\Delta^{199}Hg_{GEM}$ and

388       $\Delta^{200}Hg_{GEM}$ remained unchanged. The $\delta^{202}Hg_{GEM}$ was up to 0.91‰ during the most pronounced

389   depletion event (on 13 Jul 2013, daily mean GEM of 0.91 ng m^{-3}), 1.05‰ higher than the values

390   at the beginning and end of the sampling period (on 9 and 17 Jul 2013, mean GEM = 1.57 - 1.60

391   ng m^{-3}, mean $\delta^{202}Hg_{GEM}$ = -0.14‰). The $\delta^{202}Hg_{GEM}$ values were anti-correlated with GEM

392   concentrations (r^2 = 0.58, $p < 0.01$), whereas no clear relationship can be established between

393       $\Delta^{199}Hg$, and $\Delta^{200}Hg_{GEM}$ values and atmospheric GEM concentrations (p values for both > 0.05).

394   The lower $\delta^{202}Hg_{GEM}$ values at the beginning and end of the sampling period were likely

395   representative of the regional background $\delta^{202}Hg_{GEM}$ signatures as the GEM concentrations of

396   the two samples were close to the long-term GEM mean concentration at Mt. Changbai, whereas

397   the positive $\delta^{202}Hg_{GEM}$ shifts during 11 - 15 Jul 2013 were most likely due to the uptake of GEM

398   by forest foliage which has been known to induce mass dependent fractionation (MDF, $\delta^{202}Hg$

399   signature) and negligible MIF($\Delta^{199}Hg$, $\Delta^{200}Hg$ signatures) of Hg isotopes (Demers et al.,

400   2013;Enrico et al., 2016). MDF and MIF of Hg isotopes caused by GEM oxidation have not

401   been well characterized. Studies observed both significant MDF and MIF of Hg isotopes during

402   aqueous- and gas-phase chemical oxidation of elemental Hg (Stathopoulos, 2014;Sun et al.,

403   2016). Our study at Pic du Midi, France (2877 m above sea level) also observed clear shifts of

404       $\delta^{202}Hg_{GEM}$ and $\Delta^{199}Hg_{GEM}$ during oxidation of GEM to GOM, indicating both MDF and MIF

405   could occur during 'net oxidation' of GEM in the ambient air (Sonke *et al.*, manuscript under

406 preparation). Therefore, we conclude foliar uptake of GEM played a predominant role in the

407 GEM depletion at Mt. Changbai.

408 To answer the question whether or not GEM dry deposition to forest canopy alone can

409 explain the GEM depletion at Mt. Changbai, the forced change of GEM concentrations by

410 canopy uptake at the sampling height of 24 m under a typical NBL height of 100 m was

411 simulated using a box model (see text in the SI). The box model results suggest that complete

412 GEM depletions can be achieved by canopy uptake alone in the presence of shallow NBL and

413 low vertical turbulent diffusivity (Figure 7). With a dry deposition GEM flux of 7.3 ng m^{-2} h^{-1}

414 and turbulent diffusivity of 0.1 - 1.0 cm s^{-1} at night (Figure S6), the model predicted that GEM

415 concentrations can be decreased to nearly 0 ng m^{-3} (Figure 7). Depletion cannot occur during

416 daytime mainly due to the low dry deposition flux (~2.5 ng m^{-2} h^{-1}), high vertical turbulent

417 diffusivity (1 - 100 cm s^{-1}) and absence of shallow NBL (Figure 7). The GEM depletion event at

418 Mt. Changbai showed a seasonal trend with the depletion occurring more frequently and

419 pronouncedly during leaf-growing season from July to August. This can be attributed to: (1)

420 seasonal LAI changes (Figure S7.A), (2) lower wind speed from July to August (Figure S7.B),

421 and (3) the wind direction that inhibited the transport of polluted air from anthropogenic source

422 regions (90º-202º, natural preserve areas without significant local and regional sources) during

423 leaf-growing season (Figure S7.C). LAI is the highest in July and August (~5.4) compared to the

424 non-growing season (<2, Figure S8.A) (Shi et al., 2008). Higher LAI values indicate higher dry

425 deposition fluxes of GEM to forest canopy. The low wind speed facilitated the buildup of

426 shallow NBL.

4 Conclusions and implications for the global atmospheric Hg cycling

428 Depletions of atmospheric GEM were consistently observed during leaf-growing season in

429 Mt. Changbai forest, Northeast China. The depletions occurred exclusively at night in the

430 absence of GOM enrichments. This is in contrast to previously characterized GEM depletions in

431 the polar and sub-polar regions, marine boundary layer and free troposphere where depletions of

432   GEM were mainly caused by fast chemical oxidation of GEM to GOM followed by deposition.

433   The measurements of GEM vertical gradients, foliar GEM fluxes, atmospheric speciated Hg and

434   ambient GEM isotope compositions suggest foliar uptake of GEM played a predominant role in

435   the GEM depletion at Mt. Changbai.

436   Forests cover ~30% (~40 million km^2) of the Earth's land surface. There is a need to

437   quantitatively assess the role of global forest in global Hg cycling. Tables S3, S4, and S5

438   summarize the published data of litterfall fluxes at 68 forest sites, throughfall fluxes at 23 forest

439   sites, and emissions from forest floors at 31 forest sites in North America, Europe, Asia, and

440   South America. For the regions (Africa and Oceania) that lack observational data, it is assumed

441   that that the median values of the published data are representative. There has not been reliable

442   data on Hg emission from forest canopies via evapotranspiration. We therefore use the observed

443   xylem Hg concentrations and total evapotranspiration from the global forests to estimate Hg

444   emissions from this sector (Bishop et al., 1998;Baldocchi and Ryu, 2011).

445   Using a mass balance approach, we estimated that global inputs of Hg via litterfall and

446   throughfall were 1,232 and 1,338 Mg yr^{-1}, respectively. Hg emissions via the evasion from soil

447   and plant evapotranspiration were 381 and 260 Mgyr^{-1}, respectively. Combining the source and

448   sink terms, the global forest ecosystem represents a net sink of ~1,930 Mg yr^{-1} of atmospheric

449   Hg. The value is much larger than the estimate of Hg uptake by forest above-ground biomass

450   (Obrist, 2007). The estimate by Obrist (2007) did not include deposition flux by throughfall; and

451   the Hg concentration in biomass used in the study was 2 - 10 times lower than the measured Hg

452   contents in North America, Europe, China and South America (Lindberg et al., 2007;Obrist,

453   2007;Risch et al., 2012;Teixeira et al., 2012;Fu et al., 2015). Our estimate is comparable to the

454   upper limit of atmospheric Hg deposition to terrestrial ecosystem predicted by modeling studies

455   (800-1900 Mg) (Mason and Sheu, 2002;Holmes et al., 2010;Driscoll et al., 2013). This implies

456   that forest ecosystem may be the largest sink of atmospheric Hg in the terrestrial ecosystems,

457   whereas other terrestrial ecosystems may represent net sources.

458   **Supporting Information:**

459 Descriptions of the simulation of NBL, turbulent diffusivity and the box model are shown

460 in supplementary text. The location of the Mt. Changbai forest, GEM concentrations at 4 m agl

461 in a small clearing plot and 24 m and 45 m agl, diurnal trends in vertical GEM gradient, soil/air

462 GEM flux, diurnal variations of meteorological parameters, turbulent diffusivity and seasonal

463 variations in LAI, wind speed and wind direction at Mt. Changbai forest are shown in Figure

464 S1-S7. Littefall Hg concentrations and litter mass at Mt. Changbai forest, isotopic composition

465 of atmospheric GEM as well as compiled litterfall and throughfall Hg deposition fluxes, and

466 forest soil/air GEM fluxes over the global forests are shown in Table S1-S5.

467 **Acknowledgements.** This work was funded by the National "973" Program of China (2013CB430003); the

468 National Science Foundation of China (41473025, 41273145, and 41428301) and Guangzhou Science and

469 Technology Projects (2014J4100089). We acknowledge Alexandra Steffen from Environment Canada for

470 offering the sampling instruments, Open Research Station of Changbai Mountain Forest Ecosystems for the

471 meteorological parameters and field sampling, CAS, and Hao Xu for assistance with field sampling. The data

472 used are listed in the references, tables, and supplements.

References

474 Amos, H. M., Jacob, D. J., Streets, D. G., and Sunderland, E. M.: Legacy impacts of all-time anthropogenic
475 emissions on the global mercury cycle, Global Biogeochem Cy, 27, 410-421, 10.1002/gbc.20040, 2013.
476 Baldocchi, D., and Ryu, Y.: A Synthesis of Forest Evaporation Fluxes – from Days to Years – as Measured with
477 Eddy Covariance, in: Forest Hydrology and Biogeochemistry, edited by: Levia, D. F., Carlyle-Moses, D., and
478 Tanaka, T., Ecological Studies, Springer Netherlands, 101-116, 2011.
479 Bash, J. O., and Miller, D. R.: Growing season total gaseous mercury (TGM) flux measurements over an Acer
480 rubrum L. stand, Atmos Environ, 43, 5953-5961, DOI 10.1016/j.atmosenv.2009.08.008, 2009.
481 Bishop, K. H., Lee, Y. H., Munthe, J., and Dambrine, E.: Xylem sap as a pathway for total mercury and
482 methylmercury transport from soils to tree canopy in the boreal forest, Biogeochemistry, 40, 101-113, 1998.
483 Biswas, A., Blum, J. D., Bergquist, B. A., Keeler, G. J., and Xie, Z. Q.: Natural mercury isotope variation in coal
484 deposits and organic soils, Environmental Science & Technology, 42, 8303-8309, Doi 10.1021/Es801444b, 2008.
485 Blum, J. D., and Bergquist, B. A.: Reporting of variations in the natural isotopic composition of mercury, Anal
486 Bioanal Chem, 388, 353-359, DOI 10.1007/s00216-007-1236-9, 2007.
487 Brunke, E. G., Labuschagne, C., Ebinghaus, R., Kock, H. H., and Slemr, F.: Gaseous elemental mercury depletion
488 events observed at Cape Point during 2007-2008, Atmos Chem Phys, 10, 1121-1131, 2010.
489 Dai, L. M., Qi, L., Wang, Q. W., Su, D. K., Yu, D. P., Wang, Y., Ye, Y. J., Jiang, S. W., and Zhao, W.: Changes in
490 forest structure and composition on Changbai Mountain in Northeast China, Ann Forest Sci, 68, 889-897, DOI
491 10.1007/s13595-011-0095-x, 2011.

492 Demers, J. D., Blum, J. D., and Zak, D. R.: Mercury isotopes in a forested ecosystem: Implications for air-surface
493 exchange dynamics and the global mercury cycle, Global Biogeochem Cy, 27, 222-238, Doi 10.1002/Gbc.20021,
494 2013.
495 Demers, J. D., Sherman, L. S., Blum, J. D., Marsik, F. J., and Dvonch, J. T.: Coupling atmospheric mercury isotope
496 ratios and meteorology to identify sources of mercury impacting a coastal urban-industrial region near Pensacola,
497 Florida, USA, Global Biogeochem Cy, 29, 1689-1705, 2015.
498 Driscoll, C. T., Mason, R. P., Chan, H. M., Jacob, D. J., and Pirrone, N.: Mercury as a Global Pollutant: Sources,
499 Pathways, and Effects, Environmental Science & Technology, 47, 4967-4983, Doi 10.1021/Es305071v, 2013.
500 Ebinghaus, R., Kock, H. H., Temme, C., Einax, J. W., Lowe, A. G., Richter, A., Burrows, J. P., and Schroeder, W. H.:
501 Antarctic springtime depletion of atmospheric mercury, Environmental Science & Technology, 36, 1238-1244, Doi
502 10.1021/Es015710z, 2002.
503 Enrico, M., Le Roux, G., Marusczak, N., Heimburger, L. E., Claustres, A., Fu, X. W., Sun, R. Y., and Sonke, J. E.:
504 Atmospheric Mercury Transfer to Peat Bogs Dominated by Gaseous Elemental Mercury Dry Deposition,
505 Environmental Science & Technology, 50, 2405-2412, 10.1021/acs.est.5b06058, 2016.
506 Ericksen, J. A., Gustin, M. S., Schorran, D. E., Johnson, D. W., Lindberg, S. E., and Coleman, J. S.: Accumulation
507 of atmospheric mercury in forest foliage, Atmos Environ, 37, 1613-1622, 2003.
508 Ericksen, J. A., and Gustin, M. S.: Foliar exchange of mercury as a function of soil and air mercury concentrations,
509 Sci Total Environ, 324, 271-279, DOI 10.1016/j.scitotenv.200310.034, 2004.
510 Fain, X., Obrist, D., Hallar, A. G., Mccubbin, I., and Rahn, T.: High levels of reactive gaseous mercury observed at a
511 high elevation research laboratory in the Rocky Mountains, Atmos Chem Phys, 9, 8049-8060, 2009.
512 Finkelstein, P. L., Ellestad, T. G., Clarke, J. F., Meyers, T. P., Schwede, D. B., Hebert, E. O., and Neal, J. A.: Ozone
513 and sulfur dioxide dry deposition to forests: Observations and model evaluation, J Geophys Res-Atmos, 105,
514 15365-15377, Doi 10.1029/2000jd900185, 2000.
515 Frescholtz, T. F., and Gustin, M. S.: Soil and foliar mercury emission as a function of soil concentration, Water Air
516 Soil Poll, 155, 223-237, Doi 10.1023/B:Wate.0000026530.85954.3f, 2004.
517 Fu, X. W., Sonke, J. E., and Heimbürger, L.-E.: Collection of atmospheric gaseous mercury for stable isotope
518 analysis using iodine- and chlorine-impregnated activated carbon traps, J Anal Atom Spectrom, In review, 2014.
519 Fu, X. W., Zhang, H., Yu, B., Wang, X., Lin, C. J., and Feng, X. B.: Observations of atmospheric mercury in China:
520 a critical review, Atmos. Chem. Phys., 15, 9455-9476, 10.5194/acp-15-9455-2015, 2015.
521 Fu, X. W., Marusczak, N., Heimburger, L. E., Sauvage, B., Gheusi, F., Prestbo, E. M., and Sonke, J. E.: Atmospheric
522 mercury speciation dynamics at the high-altitude Pic du Midi Observatory, southern France, Atmos. Chem. Phys.,
523 16, 5623-5639, 10.5194/acp-16-5623-2016, 2016.
524 Gratz, L. E., Keeler, G. J., Blum, J. D., and Sherman, L. S.: Isotopic composition and fractionation of mercury in
525 Great Lakes precipitation and ambient air, Environmental Science & Technology, 44, 7764-7770, Doi
526 10.1021/Es100383w, 2010.
527 Graydon, J. A., St Louis, V. L., Lindberg, S. E., Hintelmann, H., and Krabbenhoft, D. P.: Investigation of mercury
528 exchange between forest canopy vegetation and the atmosphere using a new dynamic chamber, Environmental
529 Science & Technology, 40, 4680-4688, Doi 10.1021/Es0604616, 2006.
530 Gustin, M., and Jaffe, D.: Reducing the Uncertainty in Measurement and Understanding of Mercury in the
531 Atmosphere, Environmental Science & Technology, 44, 2222-2227, Doi 10.1021/Es902736k, 2010.
532 Gustin, M. S., Ericksen, J. A., Schorran, D. E., Johnson, D. W., Lindberg, S. E., and Coleman, J. S.: Application of

533   controlled mesocosms for understanding mercury air-soil-plant exchange, Environmental Science & Technology, 38,
534   6044-6050, Doi 10.1021/Es0487933, 2004.

535   Gustin, M. S., Huang, J. Y., Miller, M. B., Peterson, C., Jaffe, D. A., Ambrose, J., Finley, B. D., Lyman, S. N., Call,
536   K., Talbot, R., Feddersen, D., Mao, H. T., and Lindberg, S. E.: Do we understand what the mercury speciation
537   instruments are actually measuring? Results of RAMIX, Environmental Science & Technology, 47, 7295-7306, Doi
538   10.1021/Es3039104, 2013.

539   Gustin, M. S., Amos, H. M., Huang, J., Miller, M. B., and Heidecorn, K.: Measuring and modeling mercury in the
540   atmosphere: a critical review, Atmos Chem Phys, 15, 5697-5713, DOI 10.5194/acp-15-5697-2015, 2015.

541   Hanson, P. J., Lindberg, S. E., Tabberer, T. A., Owens, J. G., and Kim, K. H.: Foliar Exchange of Mercury-Vapor -
542   Evidence for a Compensation Point, Water Air Soil Poll, 80, 373-382, Doi 10.1007/Bf01189687, 1995.

543   Hens, K., Novelli, A., Martinez, M., Auld, J., Axinte, R., Bohn, B., Fischer, H., Keronen, P., Kubistin, D., Nolscher,
544   A. C., Oswald, R., Paasonen, P., Petaja, T., Regelin, E., Sander, R., Sinha, V., Sipila, M., Taraborrelli, D., Ernest, C.
545   T., Williams, J., Lelieveld, J., and Harder, H.: Observation and modelling of HOx radicals in a boreal forest, Atmos
546   Chem Phys, 14, 8723-8747, 10.5194/acp-14-8723-2014, 2014.

547   Holmes, C. D., Jacob, D. J., Corbitt, E. S., Mao, J., Yang, X., Talbot, R., and Slemr, F.: Global atmospheric model
548   for mercury including oxidation by bromine atoms, Atmos Chem Phys, 10, 12037-12057, DOI
549   10.5194/acp-10-12037-2010, 2010.

550   Huang, J. Y., Miller, M. B., Weiss-Penzias, P., and Gustin, M. S.: Comparison of gaseous oxidized Hg measured by
551   KCl-coated denuders, and Nylon and Cation exchange Membranes, Environmental Science & Technology, 47,
552   7307-7316, Doi 10.1021/Es4012349, 2013.

553   Huang, J. Y., and Gustin, M. S.: Use of Passive Sampling Methods and Models to Understand Sources of Mercury
554   Deposition to High Elevation Sites in the Western United States, Environmental Science & Technology, 49, 432-441,
555   10.1021/es502836w, 2015.

556   Kim, K. H., Lindberg, S. E., and Meyers, T. P.: Micrometeorological Measurements of Mercury-Vapor Fluxes over
557   Background Forest Soils in Eastern Tennessee, Atmos Environ, 29, 267-282, Doi 10.1016/1352-2310(94)00198-T,
558   1995.

559   Lan, X., Talbot, R., Castro, M., Perry, K., and Luke, W.: Seasonal and diurnal variations of atmospheric mercury
560   across the US determined from AMNet monitoring data, Atmos Chem Phys, 12, 10569-10582, DOI
561   10.5194/acp-12-10569-2012, 2012.

562   Landis, M. S., Stevens, R. K., Schaedlich, F., and Prestbo, E. M.: Development and characterization of an annular
563   denuder methodology for the measurement of divalent inorganic reactive gaseous mercury in ambient air,
564   Environmental Science & Technology, 36, 3000-3009, Doi 10.1021/Es015887t, 2002.

565   Lindberg, S., Bullock, R., Ebinghaus, R., Engstrom, D., Feng, X. B., Fitzgerald, W., Pirrone, N., Prestbo, E., and
566   Seigneur, C.: A synthesis of progress and uncertainties in attributing the sources of mercury in deposition, Ambio,
567   36, 19-32, 2007.

568   Lindberg, S. E., Hanson, P. J., Meyers, T. P., and Kim, K. H.: Air/surface exchange of mercury vapor over forests -
569   The need for a reassessment of continental biogenic emissions, Atmos Environ, 32, 895-908, Doi
570   10.1016/S1352-2310(97)00173-8, 1998.

571   Lindberg, S. E., and Stratton, W. J.: Atmospheric mercury speciation: Concentrations and behavior of reactive
572   gaseous mercury in ambient air, Environmental Science & Technology, 32, 49-57, Doi 10.1021/Es970546u, 1998.

573   Lindberg, S. E., Brooks, S., Lin, C. J., Scott, K. J., Landis, M. S., Stevens, R. K., Goodsite, M., and Richter, A.:

574 Dynamic oxidation of gaseous mercury in the Arctic troposphere at polar sunrise, Environmental Science &
575 Technology, 36, 1245-1256, Doi 10.1021/Es0111941, 2002.

576 Lyman, S. N., and Jaffe, D. A.: Formation and fate of oxidized mercury in the upper troposphere and lower
577 stratosphere, Nat Geosci, 5, 114-117, Doi 10.1038/Ngeo1353, 2012.

578 Mao, H., Talbot, R. W., Sigler, J. M., Sive, B. C., and Hegarty, J. D.: Seasonal and diurnal variations of Hg degrees
579 over New England, Atmos Chem Phys, 8, 1403-1421, 2008.

580 Mason, R. P., and Sheu, G. R.: Role of the ocean in the global mercury cycle, Global Biogeochem Cy, 16, Artn 1093
581 Doi 10.1029/2001gb001440, 2002.

582 Millhollen, A. G., Gustin, M. S., and Obrist, D.: Foliar mercury accumulation and exchange for three tree species,
583 Environmental Science & Technology, 40, 6001-6006, Doi 10.1021/Es0609194, 2006.

584 Munger, J. W., Wofsy, S. C., Bakwin, P. S., Fan, S. M., Goulden, M. L., Daube, B. C., Goldstein, A. H., Moore, K.
585 E., and Fitzjarrald, D. R.: Atmospheric deposition of reactive nitrogen oxides and ozone in a temperate deciduous
586 forest and a subarctic woodland .1. Measurements and mechanisms, J Geophys Res-Atmos, 101, 12639-12657, Doi
587 10.1029/96jd00230, 1996.

588 Obrist, D.: Atmospheric mercury pollution due to losses of terrestrial carbon pools?, Biogeochemistry, 85, 119-123,
589 DOI 10.1007/s10533-007-9108-0, 2007.

590 Obrist, D., Tas, E., Peleg, M., Matveev, V., Fain, X., Asaf, D., and Luria, M.: Bromine-induced oxidation of mercury
591 in the mid-latitude atmosphere, Nat Geosci, 4, 22-26, Doi 10.1038/Ngeo1018, 2011.

592 Pan, Y. D., Birdsey, R. A., Fang, J. Y., Houghton, R., Kauppi, P. E., Kurz, W. A., Phillips, O. L., Shvidenko, A.,
593 Lewis, S. L., Canadell, J. G., Ciais, P., Jackson, R. B., Pacala, S. W., McGuire, A. D., Piao, S. L., Rautiainen, A.,
594 Sitch, S., and Hayes, D.: A Large and Persistent Carbon Sink in the World's Forests, Science, 333, 988-993, DOI
595 10.1126/science.1201609, 2011.

596 Poissant, L., Pilote, M., Yumvihoze, E., and Lean, D.: Mercury concentrations and foliage/atmosphere fluxes in a
597 maple forest ecosystem in Quebec, Canada, J Geophys Res-Atmos, 113, Artn D10307
598 Doi 10.1029/2007jd009510, 2008.

599 Rea, A. W., Lindberg, S. E., and Keeler, G. J.: Assessment of dry deposition and foliar leaching of mercury and
600 selected trace elements based on washed foliar and surrogate surfaces, Environmental Science & Technology, 34,
601 2418-2425, 10.1021/es991305k, 2000.

602 Rinne, J., Markkanen, T., Ruuskanen, T. M., Petaja, T., Keronen, P., Tang, M. J., Crowley, J. N., Rannik, U., and
603 Vesala, T.: Effect of chemical degradation on fluxes of reactive compounds - a study with a stochastic Lagrangian
604 transport model, Atmos Chem Phys, 12, 4843-4854, 10.5194/acp-12-4843-2012, 2012.

605 Risch, M. R., DeWild, J. F., Krabbenhoft, D. P., Kolka, R. K., and Zhang, L. M.: Litterfall mercury dry deposition in
606 the eastern USA, Environ Pollut, 161, 284-290, DOI 10.1016/j.envpol.2011.06.005, 2012.

607 Schroeder, W. H., Anlauf, K. G., Barrie, L. A., Lu, J. Y., Steffen, A., Schneeberger, D. R., and Berg, T.: Arctic
608 springtime depletion of mercury, Nature, 394, 331-332, Doi 10.1038/28530, 1998.

609 Selin, N. E., Jacob, D. J., Park, R. J., Yantosca, R. M., Strode, S., Jaegle, L., and Jaffe, D.: Chemical cycling and
610 deposition of atmospheric mercury: Global constraints from observations, J Geophys Res-Atmos, 112, Artn D02308
611 Doi 10.1029/2006jd007450, 2007.

612 Selin, N. E., Jacob, D. J., Yantosca, R. M., Strode, S., Jaegle, L., and Sunderland, E. M.: Global 3-D
613 land-ocean-atmosphere model for mercury: Present-day versus preindustrial cycles and anthropogenic enrichment
614 factors for deposition, Global Biogeochem Cy, 22, Artn Gb2011

615 10.1029/2007gb003040, 2008.

616 Shah, V., Jaegle, L., Gratz, L. E., Ambrose, J. L., Jaffe, D. A., Selin, N. E., Song, S., Campos, T. L., Flocke, F. M.,

617 Reeves, M., Stechman, D., Stell, M., Festa, J., Stutz, J., Weinheimer, A. J., Knapp, D. J., Montzka, D. D., Tyndall, G.

618 S., Apel, E. C., Hornbrook, R. S., Hills, A. J., Riemer, D. D., Blake, N. J., Cantrell, C. A., and Mauldin, R. L.:

619 Origin of oxidized mercury in the summertime free troposphere over the southeastern US, Atmos Chem Phys, 16,

620 1511-1530, 10.5194/acp-16-1511-2016, 2016.

621 Sherman, L. S., Blum, J. D., Johnson, K. P., Keeler, G. J., Barres, J. A., and Douglas, T. A.: Mass-independent

622 fractionation of mercury isotopes in Arctic snow driven by sunlight, Nat Geosci, 3, 173-177, Doi 10.1038/Ngeo758,

623 2010.

624 Sheu, G. R., Lin, N. H., Wang, J. L., Lee, C. T., Yang, C. F. O., and Wang, S. H.: Temporal distribution and potential

625 sources of atmospheric mercury measured at a high-elevation background station in Taiwan, Atmos Environ, 44,

626 2393-2400, DOI 10.1016/j.atmosenv.2010.04.009, 2010.

627 Shi, T. T., Guan, D. X., Wang, A. Z., Wu, J. B., Jin, C. J., and Han, S. J.: Comparison of three models to estimate

628 evapotranspiration for a temperate mixed forest, Hydrol Process, 22, 3431-3443, 10.1002/hyp.6922, 2008.

629 Sommar, J., Zhu, W., Lin, C. J., and Feng, X. B.: Field Approaches to Measure Hg Exchange Between Natural

630 Surfaces and the Atmosphere A Review, Crit Rev Env Sci Tec, 43, 1657-1739, Doi 10.1080/10643389.2012.671733,

631 2013.

632 Spivakovsky, C. M., Logan, J. A., Montzka, S. A., Balkanski, Y. J., Foreman-Fowler, M., Jones, D. B. A., Horowitz,

633 L. W., Fusco, A. C., Brenninkmeijer, C. A. M., Prather, M. J., Wofsy, S. C., and McElroy, M. B.: Three-dimensional

634 climatological distribution of tropospheric OH: Update and evaluation, J Geophys Res-Atmos, 105, 8931-8980, Doi

635 10.1029/1999jd901006, 2000.

636 Stamenkovic, J., and Gustin, M. S.: Nonstomatal versus Stomatal Uptake of Atmospheric Mercury, Environmental

637 Science & Technology, 43, 1367-1372, Doi 10.1021/Es801583a, 2009.

638 Stathopoulos, D.: Fractionation of mercury isotopes in an aqueous environment: Chemical Oxidation. , Master

639 Dissertation, Trent University, Peterborough, Ontario, Canada, 2014.

640 Steffen, A., Douglas, T., Amyot, M., Ariya, P., Aspmo, K., Berg, T., Bottenheim, J., Brooks, S., Cobbett, F., Dastoor,

641 A., Dommergue, A., Ebinghaus, R., Ferrari, C., Gardfeldt, K., Goodsite, M. E., Lean, D., Poulain, A. J., Scherz, C.,

642 Skov, H., Sommar, J., and Temme, C.: A synthesis of atmospheric mercury depletion event chemistry in the

643 atmosphere and snow, Atmos Chem Phys, 8, 1445-1482, 2008.

644 Strode, S. A., Jaegle, L., Selin, N. E., Jacob, D. J., Park, R. J., Yantosca, R. M., Mason, R. P., and Slemr, F.: Air-sea

645 exchange in the global mercury cycle, Global Biogeochem Cy, 21, Artn Gb1017

646 Doi 10.1029/2006gb002766, 2007.

647 Sun, G. Y., Sommar, J., Feng, X. B., Lin, C. J., Ge, M. F., Wang, W. G., Fu, X. W., and Shang, L. H.: Mass

648 -dependent and -independent fractionation of mercury isotope during gas-phase oxidation of elemental mercury

649 vapor by atomic Cl and Br, Environmental Science & Technology, under revision, 2016.

650 Sun, R. Y., Enrico, M., Heimburger, L. E., Scott, C., and Sonke, J. E.: A double-stage tube furnace-acid-trapping

651 protocol for the pre-concentration of mercury from solid samples for isotopic analysis, Anal Bioanal Chem, 405,

652 6771-6781, DOI 10.1007/s00216-013-7152-2, 2013.

653 Swartzendruber, P. C., Jaffe, D. A., Prestbo, E. M., Weiss-Penzias, P., Selin, N. E., Park, R., Jacob, D. J., Strode, S.,

654 and Jaegle, L.: Observations of reactive gaseous mercury in the free troposphere at the Mount Bachelor Observatory,

655 J Geophys Res-Atmos, 111, D24301, doi 10.1029/2006jd007415, Artn D24302

656   Doi 10.1029/2006jd007415, 2006.

657   Swartzendruber, P. C., Jaffe, D. A., and Finley, B.: Improved fluorescence peak integration in the Tekran 2537 for

658   applications with sub-optimal sample loadings, Atmos Environ, 43, 3648-3651, 10.1016/j.atmosenv.2009.02.063,

659   2009a.

660   Swartzendruber, P. C., Jaffe, D. A., and Finley, B.: Development and First Results of an Aircraft-Based, High Time

661   Resolution Technique for Gaseous Elemental and Reactive (Oxidized) Gaseous Mercury, Environmental Science &

662   Technology, 43, 7484-7489, Doi 10.1021/Es901390t, 2009b.

663   Talbot, R., Mao, H. T., and Sive, B.: Diurnal characteristics of surface level O-3 and other important trace gases in

664   New England, J Geophys Res-Atmos, 110, 2005.

665   Teixeira, D. C., Montezuma, R. C., Oliveira, R. R., and Silva, E. V.: Litterfall mercury deposition in Atlantic forest

666   ecosystem from SE - Brazil, Environ Pollut, 164, 11-15, DOI 10.1016/j.envpol.2011.10.032, 2012.

667   Timonen, H., Ambrose, J. L., and Jaffe, D. A.: Oxidation of elemental Hg in anthropogenic and marine airmasses,

668   Atmos. Chem. Phys., 13, 2827-2836, 10.5194/acp-13-2827-2013, 2013.

669   Yang, X., Cox, R. A., Warwick, N. J., Pyle, J. A., Carver, G. D., O'Connor, F. M., and Savage, N. H.: Tropospheric

670   bromine chemistry and its impacts on ozone: A model study, J Geophys Res-Atmos, 110, Artn D23311

671   Doi 10.1029/2005jd006244, 2005.

672   Yin, R. S., Feng, X. B., and Meng, B.: Stable Mercury Isotope Variation in Rice Plants (Oryza sativa L.) from the

673   Wanshan Mercury Mining District, SW China, Environmental Science & Technology, 47, 2238-2245, Doi

674   10.1021/Es304302a, 2013.

675   Zhang, H. H., Poissant, L., Xu, X. H., and Pilote, M.: Explorative and innovative dynamic flux bag method

676   development and testing for mercury air-vegetation gas exchange fluxes, Atmos Environ, 39, 7481-7493, DOI

677   10.1016/j.atmosenv.2005.07.068, 2005.

678   Zhang, L., Blanchard, P., Gay, D. A., Prestbo, E. M., Risch, M. R., Johnson, D., Narayan, J., Zsolway, R., Holsen, T.

679   M., Miller, E. K., Castro, M. S., Graydon, J. A., St Louis, V. L., and Dalziel, J.: Estimation of speciated and total

680   mercury dry deposition at monitoring locations in eastern and central North America, Atmos Chem Phys, 12,

681   4327-4340, DOI 10.5194/acp-12-4327-2012, 2012.

682   Zhang, L. M., Gong, S. L., Padro, J., and Barrie, L.: A size-segregated particle dry deposition scheme for an

683   atmospheric aerosol module, Atmos Environ, 35, 549-560, Doi 10.1016/S1352-2310(00)00326-5, 2001.

684   Zhang, L. M., Wright, L. P., and Blanchard, P.: A review of current knowledge concerning dry deposition of

685   atmospheric mercury, Atmos Environ, 43, 5853-5864, DOI 10.1016/j.atmosenv.2009.08.019, 2009.

686   Zhou, Y., Su, J. Q., Janssens, I. A., Zhou, G. S., and Xiao, C. W.: Fine root and litterfall dynamics of three Korean

687   pine (Pinus koraiensis) forests along an altitudinal gradient, Plant Soil, 374, 19-32, DOI

688   10.1007/s11104-013-1816-8, 2014.

689

690   Figure 1. Atmospheric 5-min GEM concentrations at Mt. Changbai from Oct 2008 to Dec 2015 (leaf-growing

691   season is marked as the shaded area).
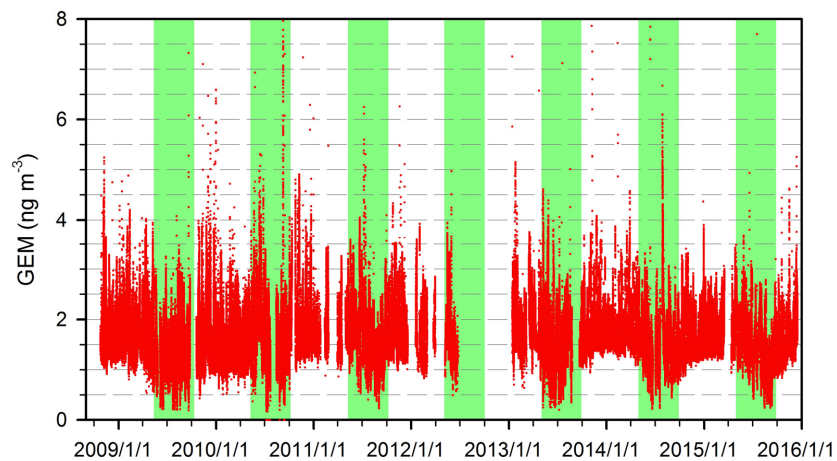
692

693

694

695   Figure 2. Time series of (A) GEM (5-min mean) and meteorological parameters from 3 to 19 July 2010 and (B)

696   speciated atmospheric Hg (GEM, GOM, and PBM) and meteorological parameters 8 to 24 July 2013

697   (nighttime is marked as the shaded area).
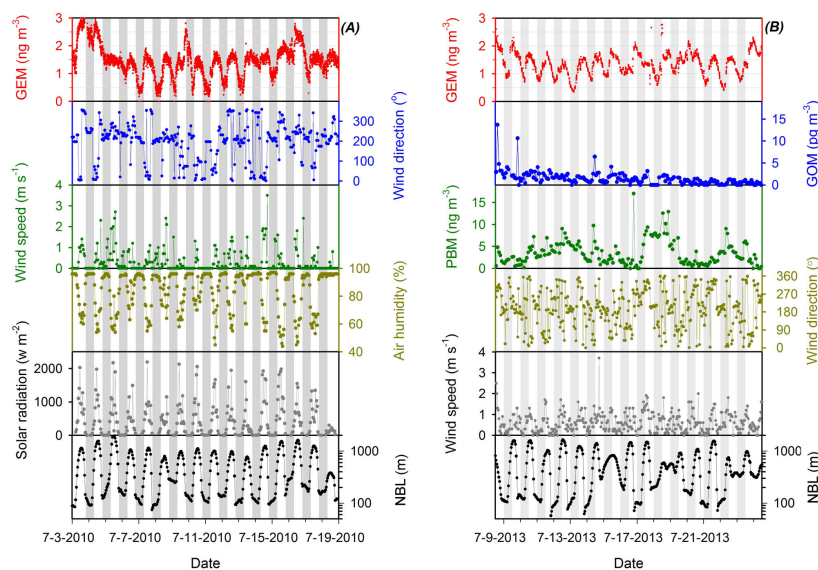
698

699

700   Figure 3. Diurnal variations of GEM concentrations at different height and metrological parameters in Mt.

701   Changbai forest from 10 to 15 July 2013 (nighttime is marked as shaded area).
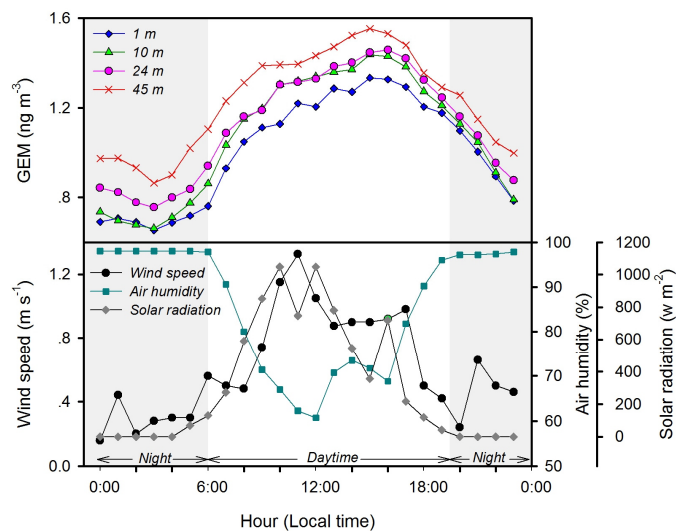
702

703

704   Figure 4. Foliar Hg flux over *Fraxinus Mandschurica* and *Pinus Koraiensis*, inlet and outlet GEM

705   concentrations from flux bag and meteorological parameters at Mt. Changbai in July 2013 (nighttime is

706   marked as the shaded area).
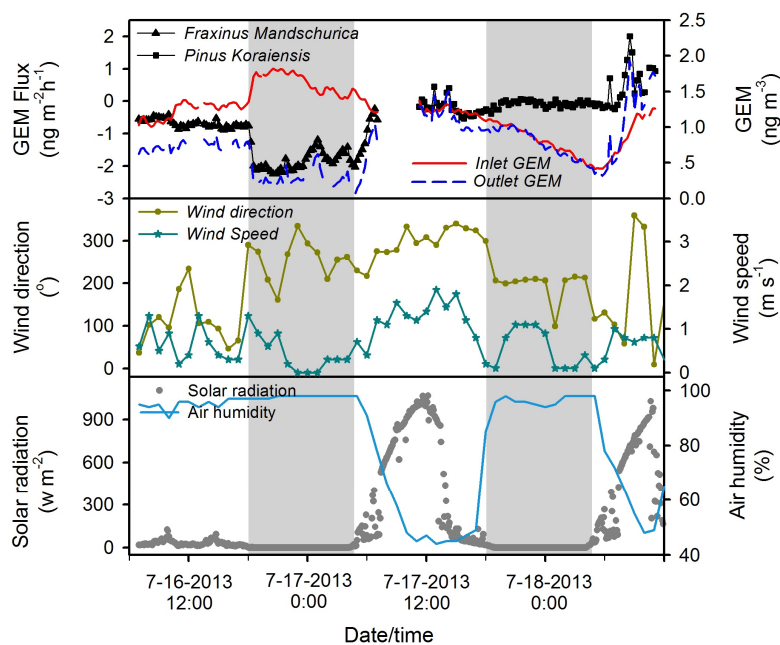
707

708

709

710   Figure 5. Daytime and nighttime correlations between atmospheric GEM concentrations and foliar GEM

711   fluxes over (A) *Fraxinus Mandschurica* and (B) *Pinus Koraiensis*.
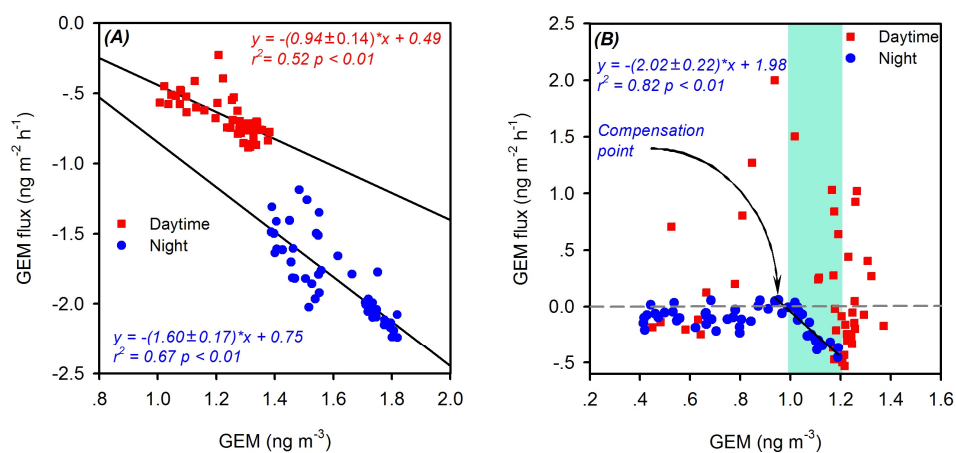
712

713

714

715   Figure 6. Temporal variation in (A) atmospheric GEM concentrations and (B) δ^{202}Hg, Δ^{199}Hg and Δ^{200}Hg

716   values of daily integrated atmospheric GEM from 9 to 18 July 2013.
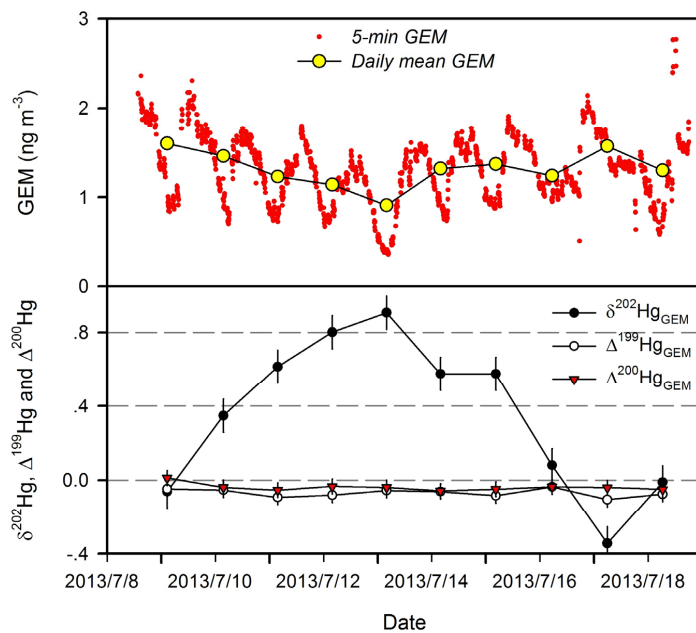
717

718

719

720

721   Figure 7. Modeling predicted variations of GEM concentration at the height of 24 m agl with dry position

722   fluxes of GEM to forest canopy and vertical turbulent diffusivity under a typical NBL height of 100 m.

723
724